Journal of *Marine Science and Engineering*

MDPI

Article

Study on the Accessibility Impact of Anti-Rolling Tank on the Offshore Wind O&M Gangway

Songtao Zhang [1,*], Peng Zhao [2,*], Chenyang Li [1], Ziqi Song [1] and Lihua Liang [1]

[1] College of Intelligent System Science and Engineering, Harbin Engineering University, Harbin 150001, China; lichenyang@hrbeu.edu.cn (C.L.); songziqi@hrbeu.edu.cn (Z.S.); lianglihua@hrbeu.edu.cn (L.L.)
[2] Department of Transportation and Vehicle Engineering, Tangshan University, Tangshan 063000, China
* Correspondence: hrbzst@126.com (S.Z.); tyjtxzp@163.com (P.Z.); Tel.: +86-13946032279 (S.Z.); +86-18733340204 (P.Z.)

Abstract: In order to improve the accessibility of offshore wind O&M gangway in complex sea conditions, a control method for the controllable anti-rolling tank based on wavelet neural network period prediction is proposed in this paper. Firstly, a model of ship motion with a controllable passive anti-rolling tank was established. Then, the inverse kinematics of the gangway were carried out. In order to analyze the influence of the anti-rolling tank on the accessibility of the on-board gangway, an accessibility simulation of the gangway under different sea conditions was completed. Finally, a hardware-in-the-loop simulation of the active compensation gangway system was carried out. The simulation and test results show that the anti-rolling tank can effectively restrain the rolling motion of the ship and significantly improve the accessibility of the on-board gangway.

Keywords: anti-rolling tank; wavelet neural network; gangway accessibility; hardware-in-the-loop simulation; roll reduction

check for updates

Citation: Zhang, S.; Zhao, P.; Li, C.; Song, Z.; Liang, L. Study on the Accessibility Impact of Anti-Rolling Tank on the Offshore Wind O&M Gangway. *J. Mar. Sci. Eng.* **2023**, *11*, 848. https://doi.org/10.3390/jmse11040848

Academic Editors: Jens Engström and Dong-Sheng Jeng

Received: 6 March 2023
Revised: 6 April 2023
Accepted: 15 April 2023
Published: 17 April 2023

1. Introduction

With the gradual depletion of fossil fuel energy and environmental pollution and other problems, countries are paying increasing attention to the development of renewable energy. The proportion of offshore wind power projects is increasing year by year with its rich resources, high utilization hours of power generation, no land occupation and suitability for large-scale development [1,2]. Accordingly, the operation and maintenance of offshore wind power equipment is also increasing.

Due to the particularity of the offshore wind power service industry, maintenance technicians need to complete their work quickly and efficiently. However, due to the interference of the marine environment, the ship will produce unexpected motion, of which rolling has the greatest impact [3]. Excessive rolling will affect the staff and mechanical performance, so it is necessary to design a special anti-rolling device to suppress rolling. Researchers and engineers have designed and manufactured a variety of passive or active anti-rolling devices to reduce ship rolling, such as a bilge keel [4], anti-rolling tanks [5], moving weights [6], Magnus rotating roll stabilizers [7,8], and fin stabilizers [3,6,9]. The rudder can also be used to reduce the roll of the ship while maintaining or changing the course [10–13]. These anti-rolling devices have their own advantages and disadvantages, but considering the application scenario of wind power operation and ship maintenance, in order to achieve anti-rolling at full speed, an anti-rolling tank is selected as the anti-rolling device to reduce ship rolling.

Zhang et al. improved the external structure of the anti-rolling tank by improving its inherent parameters [14]. Wen et al. used the MPS method based on semi-implicit moving particles to simulate the sloshing of an anti-rolling tank, and verified the applicability and reliability of the MPS method [15]. Hu used the speed and passive tank for comprehensive anti-rolling, and finally showed that the anti-rolling effect was obvious under this control

mode [16]. Luo et al. used OpenFOAM to calculate the influence of grid size, tank damping plate, and high tank liquid level on the natural period and damping parameters of a U-shaped anti-rolling tank [17]. Rahul et al. used an optimization scheme based on a genetic algorithm combined with the inherent parameter-solver of the fluid in the anti-rolling tank to optimize the main dimensions of its design [18]. Liang et al. designed a passive U-shaped anti-rolling tank with adjustable period, which showed that the tank period can be matched with the rolling period of a semi-submersible ship by controlling the baffle, so as to achieve the best anti-rolling effect of the tank [19]. Immink took the active anti-rolling tank and the gangway on the ship as the main research objects and found that the motion of the gangway on the ship was not affected by the active anti-rolling tank [20]. In view of the limitation of the lack of systematic research in the past, a combination of modelling analysis, simulation, and hardware-in-the-loop experiment is adopted to study the impact of a controllable passive anti-rolling tank on the accessibility of the offshore wind O&M gangway. Figure 1 shows the schematic diagram of an offshore wind power operation and maintenance ship equipped with an anti-rolling tank approaching the wind turbine support tower through the gangway. As shown in Figure 1, the ship may experience unexpected roll motion due to the interference of waves. Due to the limitation of the anti-rolling capability, the anti-rolling tank can only reduce a portion of the ship's roll motion. By adjusting the length of the telescopic and pitch rods installed on the gangway the remaining roll motion can be compensated as much as possible to ensure that the expected position of the end-effector remains unchanged. In this paper, the main research objective was to take the offshore wind power operation and maintenance ship, U-shaped anti-rolling tank, and gangway as the control objects, analyze and build a theoretical model of the system, and study the impact of the anti-rolling tank on gangway accessibility through simulation and semi-physical testing.

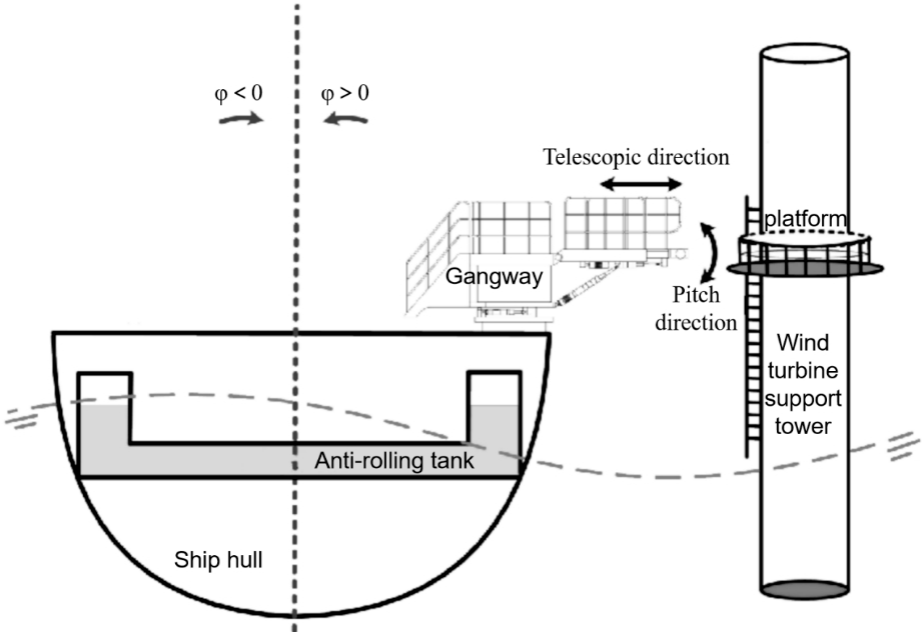

Figure 1. Schematic diagram of the ship-tank-gangway system.

The structure of the paper is as follows. Section 2 establishes the mathematical model of the ship motion with the anti-rolling tank and gangway. Sections 3 and 4 discuss and analyze the impact of the anti-rolling tank on the accessibility of the offshore wind O&M gangway through simulation and semi-physical testing. Finally, the conclusion is given.

2. Mathematical Calculations

2.1. Ship Motion Model with Controllable Passive Anti-Rolling Tank

Figure 2 shows the structural parameters of the anti-rolling tank. According to Lloyd's theory, the motion equation of the passive anti-rolling tank can be expressed as follows [21]:

$$\begin{cases} (I_{44} + a_{44})\ddot{\varphi} + b_{44}\dot{\varphi} + c_{44}\varphi + a_{4\tau}\ddot{\tau} + c_{4\tau}\tau = F_{w4} \\ a_{\tau 4}\ddot{\varphi} + c_{\tau 4}\varphi + a_{\tau\tau}\ddot{\tau} + b_{\tau\tau}\dot{\tau} + c_{\tau\tau}\tau = 0 \end{cases} \tag{1}$$

where F_{w4} represents wave interference moment; φ, $\dot{\varphi}$ and $\ddot{\varphi}$ represent the roll angle, roll angular velocity, and roll angular acceleration, respectively; τ, $\dot{\tau}$ and $\ddot{\tau}$ represent the tank level angle, angular velocity, and angular acceleration, respectively; I_{44} and a_{44} are the inertia moment and added inertia moment, respectively; b_{44} and c_{44} are damping and restoring moment coefficients, respectively; $a_{4\tau}$, $c_{4\tau}$, $a_{\tau 4}$ and $c_{\tau 4}$ are the coupling coefficients related to the inertia moment and restoring moment between ship rolling and tank, respectively and $a_{\tau\tau}$, $b_{\tau\tau}$ and $c_{\tau\tau}$ are the coefficients related to roll inertia moment, roll damping moment and roll restoring moment of the tank, respectively.

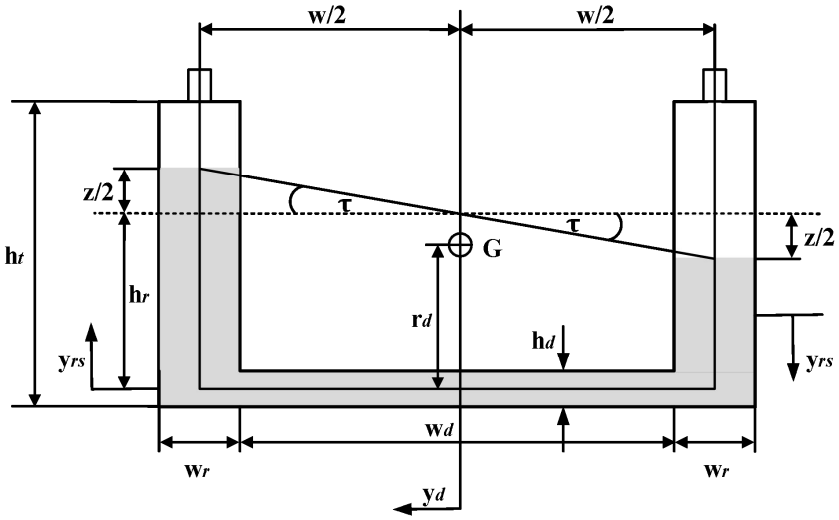

Figure 2. Structural parameters of the anti-rolling tank.

The motion equation expressed by the relative displacement z in the tank is as follows:

$$\begin{cases} (I_{44} + a_{44})\ddot{\varphi} + b_{44}\dot{\varphi} + c_{44}\varphi + \frac{a_{4\tau}}{w}\ddot{z} + \frac{c_{4\tau}}{w}z = F_{w4} \\ a_{\tau 4}\ddot{\varphi} + c_{\tau 4}\varphi + \frac{a_{\tau\tau}}{w}\ddot{z} + \frac{b_{\tau\tau}}{w}\dot{z} + \frac{c_{\tau\tau}}{w}z = 0 \end{cases} \tag{2}$$

The controllable passive anti-rolling tank should control the opening and closing of the air valve twice in each period of the ship to increase the fluid sloshing period in the tank, and make it approximately equal to the roll motion period of the ship to provide the maximum stable roll moment.

When the valve is opened, the air pressure in the chambers on both sides of the tank is equal to the atmospheric pressure, so the work done is zero, that is,

$$dU = 0 \tag{3}$$

When the valve is closed, the shaking of the liquid on both sides of the tank will cause the gas in the chamber to compress or expand. This is a variable compression process. If the relative displacement $z = z_0$ in the tank when the valve is closed, then

$$P[w_r x_t(z_1 - |z|)]^n = P_0[w_r x_t(z_1 - |z_0|)]^n \tag{4}$$

where P, P_0, and z_1 are the incident hydrostatic pressure of the side tank datum plane,

atmospheric pressure, and vertical distance from the datum plane of the side tank to the valve, respectively. n is the index of the variable compression process.

According to Equation (4), the gas pressure of the side tank with the tank level rising at any time is as follows:

$$P = P_0 \left[\frac{z_1 - |z_0|}{z_1 - |z|} \right]^n \tag{5}$$

The gas pressure of the side tank at any time when the tank level drops is as follows:

$$P = P_0 \left[\frac{z_1 + |z_0|}{z_1 + |z|} \right]^n \tag{6}$$

Then, the pressure difference between the two sides of the tank is as follows:

$$P = P_0 \left\{ \left[\frac{z_1 + |z_0|}{z_1 + |z|} \right]^n - \left[\frac{z_1 - |z_0|}{z_1 - |z|} \right]^n \right\} \tag{7}$$

Therefore, when the air valve of the controllable passive anti-rolling tank is closed, the work done by the pressure change of the side chamber on the fluid in the tank is as follows:

$$dU_2 = sign(z_0) \left\{ \left[\frac{z_1 - |z_0|}{z_1 - |z|} \right]^n - \left[\frac{z_1 - |z_0|}{z_1 - |z|} \right]^n \right\} P_0 S_0 dz \tag{8}$$

where $sign\ (\cdot)$ is a sign function.

When the air valve is opened or closed, the work of the gas pressure in the side tank of the tank is as follows:

$$dU = V sign(z_0) \left\{ \left[\frac{z_1 - |z_0|}{z_1 - |z|} \right]^n - \left[\frac{z_1 + |z_0|}{z_1 + |z|} \right]^n \right\} P_0 S_0 dz \tag{9}$$

where V is the control function. V = 0 when the air value is open, V = 1 when the air value is closed.

Then, the model of the ship with the controlled passive anti-rolling tank system can be expressed as follows [22]:

$$\begin{cases} (I_{44} + a_{44})\ddot{\varphi} + b_{44}\dot{\varphi} + c_{44}\varphi + \frac{a_{4\tau}}{w}\ddot{z} + \frac{c_{4\tau}}{w} z = F_{w4} \\ a_{\tau 4}\ddot{\varphi} + c_{\tau 4}\varphi + \frac{a_{\tau\tau}}{w}\ddot{z} + \frac{b_{\tau\tau}}{w}\dot{z} + \frac{c_{\tau\tau}}{w} z - P_0 S_0 V\, \mathrm{sign}(z_0) \left\{ \left[\frac{z_1 - |z_0|}{z_1 - |z|} \right] - \left[\frac{z_1 + |z_0|}{z_1 + |z|} \right] \right\} = 0 \end{cases} \tag{10}$$

2.2. Inverse Kinematics of Gangway

As shown in Figure 3, the function of the inverse kinematics of the gangway is to solve the change of the length of the telescopic rod ΔL_1 and the change of the length of the pitching rod ΔL_2 that keep the end effector of the gangway on the ship at the desired position when the ship rolls under the excitation of sea waves.

In Figure 3, the coordinate of the desired position of the end effector $Q(x_b, y_b)$ in the moving coordinate system X′O′Y′ is $Q'(x_b', y_b')$, and the coordinate value of the point by the coordinate system transformation is as follows:

$$x_b' = x_b \cdot \cos(-\phi) + y_b \cdot \sin(-\phi) \tag{11}$$

$$y_b' = y_b \cdot \cos(-\phi) - x_b \cdot \sin(-\phi) \tag{12}$$

The length of the gangway telescopic rod is defined as L_1', and can be expressed as follows:

$$L_1' = \sqrt{(x_b' - x_a)^2 + (y_b' - y_a)^2} \tag{13}$$

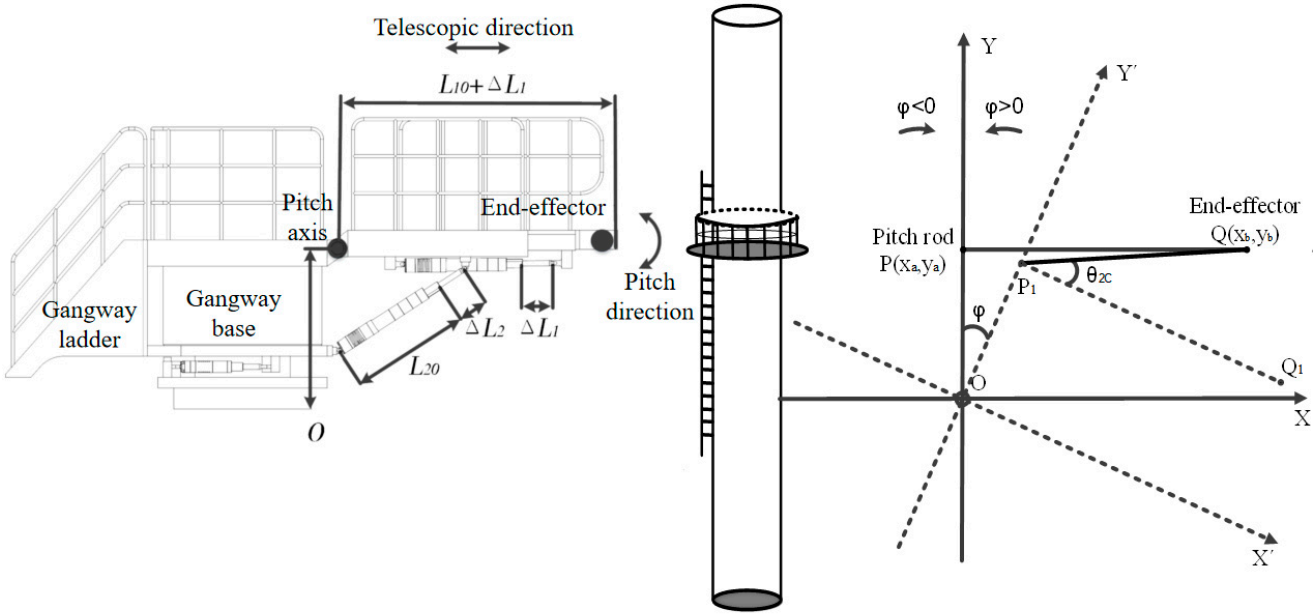

Figure 3. Gangway compensation ship rolling motion coordinate system.

When compensating for the motion of the hull, the ΔL_1 can be expressed as follows:

$$\Delta L_1 = L_1' - L_{10} = \sqrt{(x_b' - x_a)^2 + (y_b' - y_a)^2} - L_{10} \tag{14}$$

According to the trigonometric function transformation relationship, when compensating for the ship's motion, the slewing angle of the gangway is θ_{2c}, which can be expressed by the following formula:

$$\sin(\theta_{2c}) = (y_b' - y_a)/L_1' \tag{15}$$

When compensating for the hull motion, the length of the gangway pitch rod is defined as L_2'. The relationship between the length of the gangway pitch rod L_2' and the gangway rotation angle θ_{2c} is shown in Figure 4.

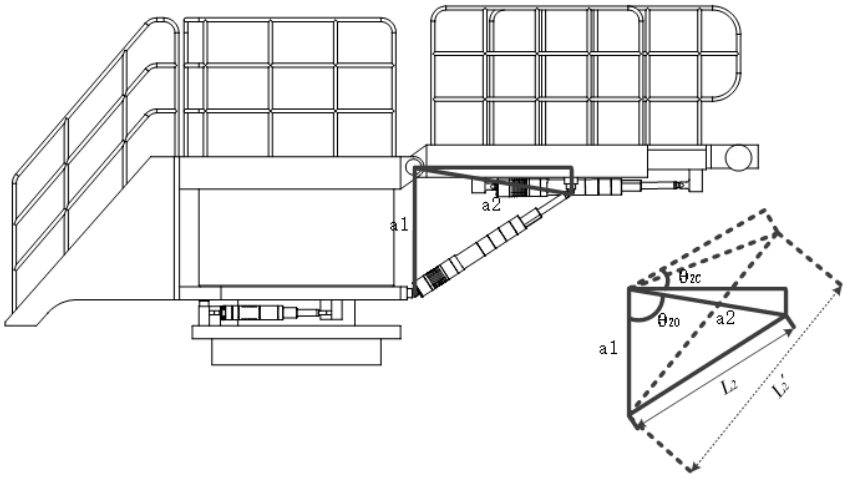

Figure 4. Relationship between the length of the pitch rod and the rotation angle.

As shown in Figure 4, the length of the pitch rod is indicated by a solid line when the gangway is not compensated for the ship motion, and the length of the pitch rod is indicated by a dotted line when the ship motion is compensated. The initial included angle between the gangway pitch rod and the vertical line of the pitch axis is θ_{20}. a_1 is the vertical distance from the pitch axis center to the static hinge point of the pitch rod, and a_2 is the

distance from the pitch axis coordinate point to the dynamic hinge point of the pitch driver. According to geometric relationship, θ_{20} can be expressed as:

$$\cos(\theta_{20}) = (a_1^2 + a_2^2 - L_2^2)/2 \cdot a_1 \cdot a_2 \tag{16}$$

Then the length of the pitch rod L_2' is as follows.

$$L_2' = \sqrt{a_1^2 + a_2^2 - 2 \cdot a_1 \cdot a_2 \cdot \cos(\theta_{20} + \theta_{2C})} \tag{17}$$

Furthermore, when compensating for the hull motion, the length change of the gangway pitch rod ΔL_2 is as follows:

$$\Delta L_2 = L_2' - L_{20} = \sqrt{a_1^2 + a_2^2 - 2 \cdot a_1 \cdot a_2 \cdot \cos(\theta_{20} + \arcsin\left[(y_b' - y_a)/\sqrt{(x_b' - x_a)^2 + (y_b' - y_a)^2}\right])} - L_{20} \tag{18}$$

2.3. Control of Air Valve

For the controllable passive anti-rolling tank, the method for selecting the control signal of the feedback valve is more critical [22]. In order to compensate for the fact that the actual tank fluid motion lags behind the ideal motion state due to the large inertia of the fluid movement in the tank, the comprehensive weighted signal of ship roll angular velocity and angular acceleration is introduced as the feedback control signal to control the controllable passive anti-rolling tank. The air valve control signal is as follows:

$$\beta = \ddot{\phi} + a\dot{\phi} \tag{19}$$

where β is the control signal and a is the weighted parameter.

If $x(t) = \dot{\phi}(t)$, the control signal can be expressed as:

$$\beta(t) = \dot{x}(t) + ax(t) \tag{20}$$

It can be seen from the above formula that the switch control signal is the linear superposition of the ship's roll angular acceleration and the ship's roll angular velocity. When the signal β changes, the air valve in the tank opens and the flow direction of the liquid in the tank changes [23].

Suppose that the rolling motion of the ship in regular wave as follows:

$$\varphi = \varphi_0 \sin(\omega_e t) \tag{21}$$

where φ_0 is the roll amplitude of the ship.

Substituting (21) into (20), the following equation can be obtained:

$$\beta = \ddot{\varphi} + a\dot{\varphi} = \varphi_0 \omega_e \sqrt{\omega_e^2 + a^2} \sin(\omega_e t - \varepsilon_\beta) \tag{22}$$

where $\varepsilon_\beta = \arctan(a/\omega_e)$ is the phase difference between the air valve control signal at the switching time and the ship roll motion.

When the air valve control signal—β is used as the control input, the fluid movement in the tank can be expressed as:

$$\tau = \tau_0 \sin(-\omega_e t + \varepsilon_\beta + \theta_0) = \tau_0 \sin(\omega_e t - \varepsilon_\beta - \theta_0 + \pi) \tag{23}$$

where τ_0 is the fluid motion amplitude in the tank and θ_0 is the phase lag caused by the inertia of the fluid in the tank. It can be seen that when $\varepsilon_\beta + \theta_0 = \pi/2$, the controllable passive anti-rolling effect is the best.

The time that the fluid in the tank flows from one side tank to the other side can be approximately equal to half of the damped oscillation period of the fluid in the tank, and the phase lag caused by the inertia of the fluid in the tank is estimated by the following formula:

$$\theta_0 = \frac{\omega_e \pi}{2\omega_{\tau d}} \tag{24}$$

where $\omega_{\tau d}$ is the damped oscillation frequency of the fluid in the tank.

3. Simulation Analysis

3.1. Hydrodynamic Simulation

A wind power operation and ship maintenance are adopted here as the research objects. The main parameters of the ship are shown in Table 1, where CG in Table 1 is the abbreviation of centre of gravity.

Table 1. Parameters of the ship.

Description	Value	Unit
Displacement	3850	ton
Water length	125	m
Beam	13.8	m
Depth	7	m
Draft	4.33	m
Height of CG	5.6	m
Metacentric height	1.5	m
Roll period	9.38	s

According to the principal dimensions of the ship in Table 1, the width of the tank is equal to about 80% of the beam of the ship to provide a large enough roll damping moment. The principal dimensions of the anti-rolling tank are listed in Table 2.

Table 2. Parameters of the anti-rolling tank.

Description	Value	Unit
Height of tank	4.4	m
Width of tank	11.23	m
Depth of tank	5.85	m
Level angle of tank	0~18	deg
Width of liquid channel	8.8	m
Width of side tank	2.44	m
Tank level height	1.93	m
Distance between CG and center line of liquid channel	3.76	m
Tank period	9.38	s
Height of liquid channel	0.75	m
Air channel number	6	-

The dimensionless damping coefficient of the water tank n_t is obtained by simulating the free and forced oscillatory motion of the fluid in the tank by Ansys Fluent, the cloud diagram of free oscillation of fluid in the tank is shown in Figure 5.

The liquid level in the left tank is set to be 3.1 m, and the liquid level in the right tank is 1.5 m. The free decay curve of the fluid in the water tank is simulated, as shown in Figure 6. According to the free decay curve, the tank period T_τ is about 8.975 s and the dimensionless damping coefficient n_t is 0.062.

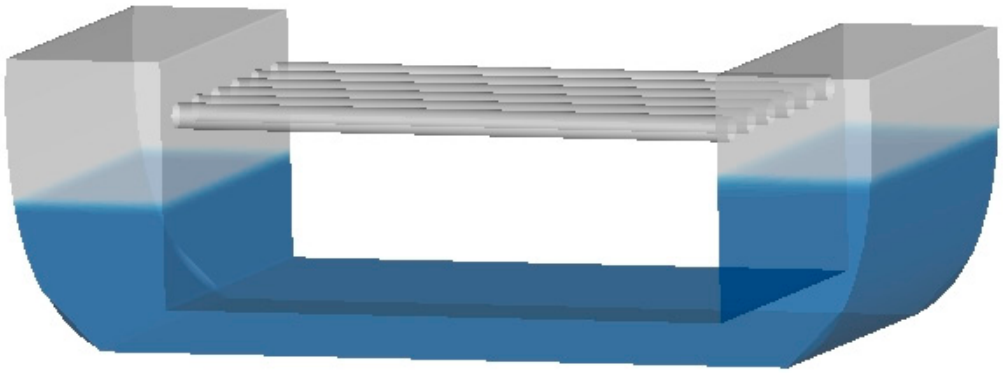

Figure 5. Cloud diagram of free oscillation of fluid in the tank.

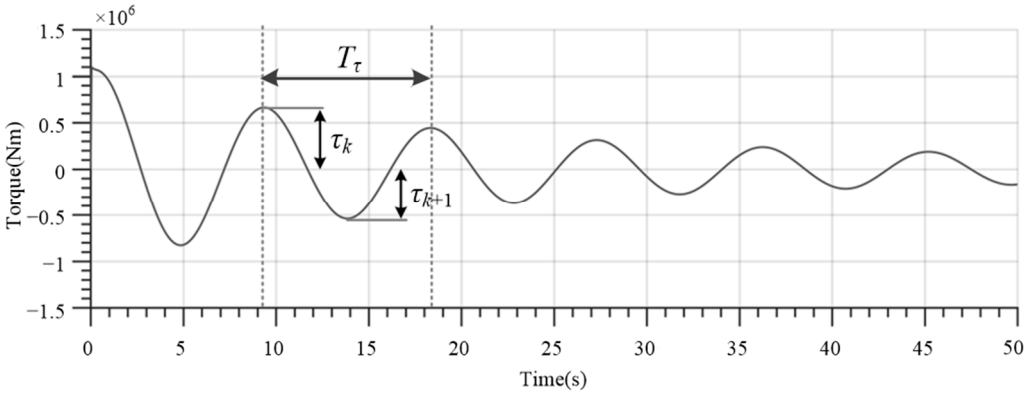

Figure 6. Free decay curve of the tank.

The designed controllable passive anti-rolling tank has six air channels. In order to study the effect of the number of air channels on the tank period and damping coefficient, free decay tests with different numbers of air channels are conducted. To facilitate the presentation of the results, the free decay curves of 1 channel and 6 channels are given here, as shown in Figure 7.

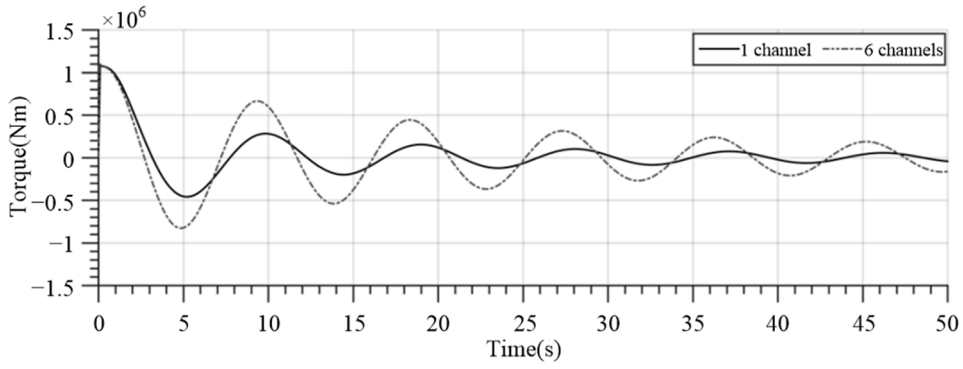

Figure 7. Free decay curves with 1 channel and 6 channels.

It can be obtained that the natural period and dimensionless damping coefficient of the tank are $T_{\tau 1}$ = 9.108 s and $n_{\tau 1}$ = 0.108, respectively, with 1 channel. The natural period and dimensionless damping coefficient of the tank are $T_{\tau 6}$ = 8.975 s and $n_{\tau 6}$ = 0.062, respectively, with 6 channels. From the simulation results, it can be seen that the valve opening has an impact on both the period and damping, but the degree of impact varies. Compared to the period and damping of 1 channel, the period and damping of 6 channels have changed by 1.46% and 42.59%, respectively. The simulation results show that the dimensionless damping coefficient of the tank increases with the decrease of the air valve opening, but has

little effect on the natural period of the tank. Compared to the tank period, the damping of the tank is more sensitive to the opening of the gas channel.

The forced oscillation simulation with 1 channel and 6 channels were carried out, and the forced oscillation curves are shown in Figure 8. The motion of the ship and the fluid in the anti-rolling tank are somewhat similar to sinusoidal and cosine motions. From the previous free decay simulation results, it can be seen that the damping of the anti-rolling tank decreases with the increase of the air valve opening. When the amplitude of ship roll motion is constant, the reduction of tank damping causes the liquid level in the side tanks to reach a higher position. Due to the fact that the anti-rolling tank provides anti-rolling force by the weight of the fluid in the side tank, the increase in liquid level in the side tank also increases the stabilizing torque that the tank can provide, to a certain extent. Consistent conclusions can be reached regarding the simulation results of forced oscillation and free decay, which mutually confirm the effectiveness of the CFD simulation and enhance the credibility of the results.

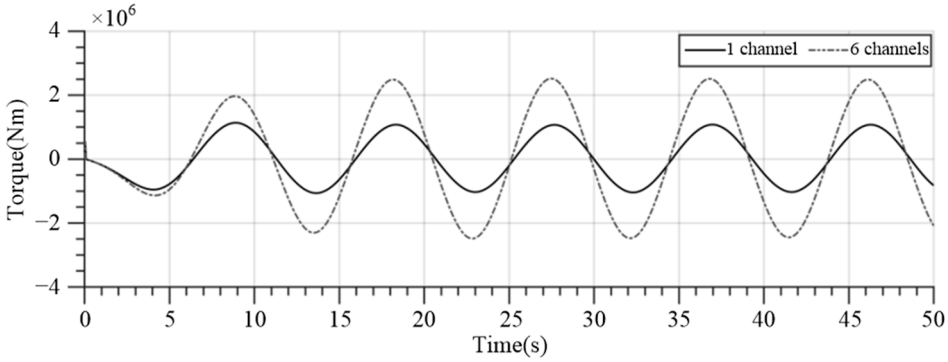

Figure 8. Forced oscillation curves with 1 channel and 6 channels.

From the above analysis of the free decay motion and forced oscillation motion simulation results of the fluid in the water tank with different air valve openings, it can be seen that the damping of the tank can be adjusted by adjusting the opening of the air valve, so as to improve the low-frequency anti-rolling phenomenon of the passive anti-rolling tank and the saturation phenomenon of the fluid in the water tank during oscillation.

3.2. Roll Period Prediction Based on Wavelet Neural Network

In order to achieve the best anti-rolling effect, it is necessary to make the natural frequency of the controllable passive anti-rolling tank equal to the ship's encounter frequency. A roll period prediction algorithm based on wavelet neural network is proposed.

The wavelet neural network is a multilayer feedforward network composed of input, hidden, and output layers [24,25]. The structure is shown in Figure 9, where X_1, X_2, ... , X_n are the input values; ω_{ij} and ω_{jk} respectively represent the weights from the input layer to the hidden layer, and from the hidden layer to the output layer; Y_1, Y_2, ... , Y_m are the output values; a_j^1 and a_k^2 are expansion factors of wavelet hidden layer and output layer basis function, respectively; and Z_j^1 and Z_k^2 represent the prediction inputs of the hidden layer and the output layer, respectively.

The wavelet basis function used in this paper is adopted as:

$$h = \cos(1.75x)e^{-x^2/2} \tag{25}$$

The input of the hidden layer and output layer of the wavelet neural network can be calculated as:

$$z_j^1 = h\left[\frac{\sum_{i=1}^{k}\omega_{ij}x_i - b_j^1}{a_j^1}\right] \quad j = 1, 2, \cdots, l \tag{26}$$

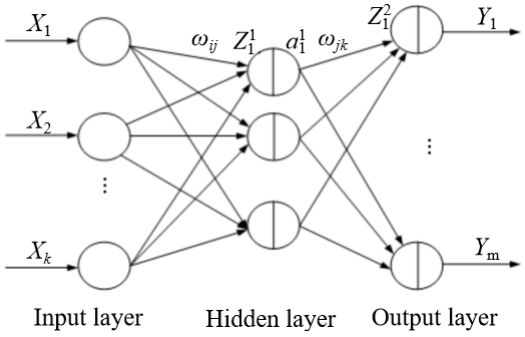

Figure 9. Structure of wavelet neural network.

$$z_k^2 = h\left[\frac{\sum_{i=1}^{k}\omega_{jk}z_j^1 - b_k^2}{a_k^2}\right] \quad k = 1, 2, \cdots, m \tag{27}$$

where b_j^1 and b_k^2 are expansion factors of the wavelet hidden layer and output layer basis function, respectively.

Define the error of the kth neuron of the output layer as e_k, and the total error of the neural network as E, then we can get:

$$e_k = \frac{1}{2}\left(Y_k - z_k^2\right)^2 \tag{28}$$

$$E = \sum e_k \tag{29}$$

The wavelet neural network uses the gradient method to modify the weights, translation factors, and expansion factors. The change of the weight from the hidden layer to the output layer and the change of the translation factor and expansion factor of the output layer can be calculated as:

$$\Delta\omega_{jk} = -\eta\frac{\partial E}{\partial\omega_{jk}} \tag{30}$$

$$\Delta a_k^2 = -\eta\frac{\partial E}{\partial a_k^2} \tag{31}$$

$$\Delta b_k^2 = -\eta\frac{\partial E}{\partial b_k^2} \tag{32}$$

The change of the weight from the input layer to the hidden layer and the change of the translation factor and expansion factor of the hidden layer can be calculated as:

$$\Delta\omega_{ij} = -\eta\frac{\partial E}{\partial\omega_{ij}} \tag{33}$$

$$\Delta a_j^1 = -\eta\frac{\partial E}{\partial a_k^1} \tag{34}$$

$$\Delta b_j^1 = -\eta\frac{\partial E}{\partial b_k^1} \tag{35}$$

Therefore, the weights, translation factors, and expansion factors can be updated as:

$$\omega_{ij} = \omega_{ij} + \Delta\omega_{ij} \tag{36}$$

$$\omega_{jk} = \omega_{jk} + \Delta\omega_{jk} \tag{37}$$

$$a_j^1 = a_j^1 + \Delta a_j^1 \tag{38}$$

$$a_k^2 = a_k^2 + \Delta a_k^2 \tag{39}$$

$$b_j^1 = b_j^1 + \Delta b_j^1 \tag{40}$$

$$b_k^2 = b_k^2 + \Delta b_k^2 \tag{41}$$

The establishment of a wavelet neural network model mainly depends on the following two aspects: selecting the number of network layers and determining the number of neuron nodes in each layer. Since the proposed roll period prediction model based on a wavelet neural network is mainly used to predict the next roll period, the number of output nodes is selected as 1. In order to improve the prediction accuracy and reduce the training time, the number of nodes in the input layer is selected as 5. The node number of the hidden layer is determined as 15, according to the experience.

By simulating the ship's rolling motion under irregular waves, a series of time sequences of the ship's rolling zero-crossing point is obtained. The roll period data can be extracted from the simulation results. The first 90% of the data is used as training samples, and the remaining 10% is used as testing data. The weight matrix ω_{ij} and ω_{jk} obtained through data training are as follows:

$$\omega_{ij} = \begin{bmatrix} 0.3700 \\ 0.2437 \\ 1.4810 \\ -0.8048 \\ -0.9134 \\ 0.4552 \\ -0.7670 \\ 0.2675 \\ 0.2528 \\ 1.0859 \\ -0.6972 \\ 0.6493 \\ -0.8433 \\ -0.2499 \\ -0.3904 \end{bmatrix}, \quad \omega_{jk} = \begin{bmatrix} 2.9207 & -0.2664 & 1.1241 & -0.3286 & -1.0107 \\ 0.9274 & -1.6937 & -0.3820 & -0.7373 & 0.1036 \\ 3.4899 & 1.3775 & -1.3275 & -2.8930 & -0.5059 \\ -1.1073 & 0.6488 & -1.0959 & -0.3198 & -0.7636 \\ -2.4833 & 0.5440 & 1.3671 & 0.5518 & 1.9224 \\ -0.5603 & -1.0031 & 0.9527 & -2.7748 & 0.8032 \\ 1.1916 & -4.001 & -1.2002 & -2.3905 & -1.0411 \\ -0.4973 & -2.3947 & 1.3754 & -1.3303 & 1.1087 \\ 3.3389 & -0.4297 & 0.5730 & 1.3572 & 2.6465 \\ -2.1497 & -0.7114 & -0.2894 & 0.1707 & -0.0897 \\ -0.2956 & -0.8925 & 0.1395 & 0.8409 & 0.0063 \\ -1.1984 & -1.0475 & -0.7609 & 0.1097 & -0.7109 \\ -0.7383 & -0.8649 & 0.0499 & 0.9869 & -0.6066 \\ 0.7588 & -2.2459 & 2.6787 & -0.2028 & -0.0704 \\ 1.2754 & 1.9865 & 2.3609 & -0.8848 & 0.9764 \end{bmatrix} \tag{42}$$

The comparison between the predicted rolling period of the wavelet neural network and the actual rolling period of the ship is shown in Figure 10. It can be seen from Figure 10 that the rolling period prediction algorithm based on WNN can predict the ship's rolling period relatively accurately.

3.3. Impact of Anti-Rolling Tank on Gangway Accessibility

Based on the dimensions of the on-board gangway, a scaled model of the gangway was made. The telescoping and pitching motions of the gangway model have their respective motion ranges due to the limitations of the mechanical structure, as shown in Table 3.

Table 3. Limitations of the gangway model.

Description	Symbol	Limitation	Unit
Length variation of telescopic rod	ΔL_1	0~50	mm
Speed of telescopic rod	v_1	±17	mm/s
Length variation of pitch rod	ΔL_2	0~50	mm
Speed of pitch rod	v_2	±17	mm/s

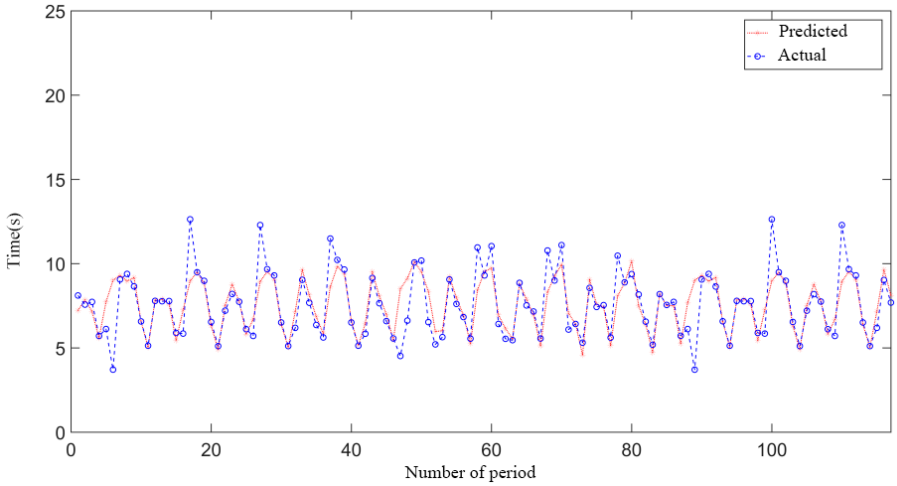

Figure 10. Comparison between predicted results and actual results of rolling period.

The gangway can compensate for a portion of the roll motion by adjusting the length of the telescopic rod and pitch rod. From the relationship between the gangway rods and the ship's roll motion, the ship's rolling limit corresponding to the gangway mechanical can be obtained. The roll angle and angular velocity limits are 4.7 deg and 0.055 rad/s, respectively.

In order to analyze the impact of the anti-rolling tank on gangway accessibility, the ship's rolling motion under different conditions is simulated and analyzed. The P-M spectrum with one parameter of the significant wave height is adopted here to simulate the wave disturbance. Considering the working scenario of the wind power operation and ship maintenance, without losing generality, the simulation conditions are set to the significant wave height of 2.5 m, corresponding to sea state 4. The speed is set to 0 kn. The simulation results of the ship's roll angle, roll angular velocity, and tank level angle are shown in Figures 11–13, respectively. The C-passive tank in the legend of Figures 11–13 represents a controllable passive anti-rolling tank.

The maximum roll response of the ship under random wave excitation is shown in Table 4. It can be seen from Figures 11–13 and Table 4 that under the same wave interference, the ship without an anti-rolling tank has the maximum roll amplitude. The controllable passive anti-rolling tank can constrain the flow of fluid inside the tank through air valves, making its anti-rolling effect superior to the passive anti-rolling tank. The tank liquid level does not exceed the limit of the maximum tank fluid angle in the event that the ship is equipped with a passive anti-rolling tank and a controllable passive anti-rolling tank.

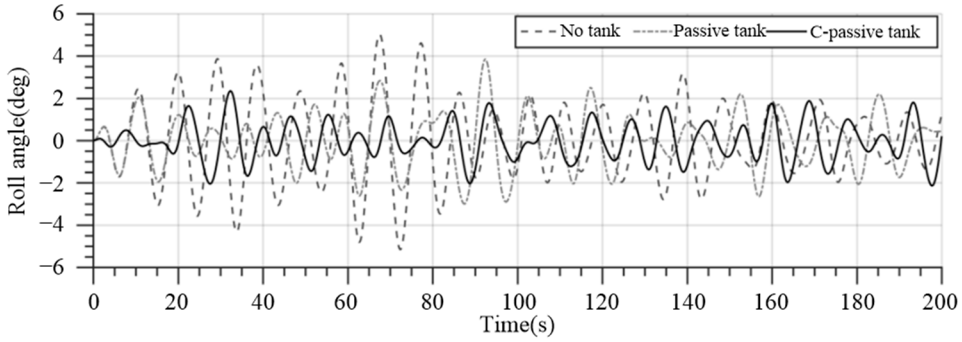

Figure 11. Roll angle of no tank, passive anti-rolling tank, and controllable passive anti-rolling tank.

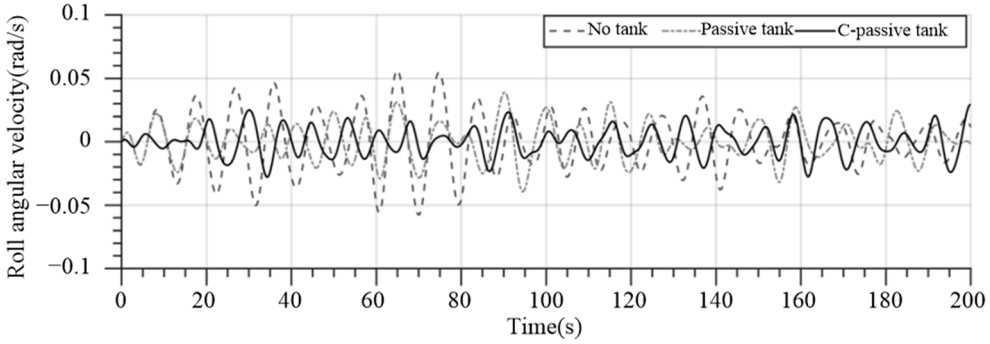

Figure 12. Roll angular velocity of no tank, passive anti-rolling tank, and controllable passive anti-rolling tank.

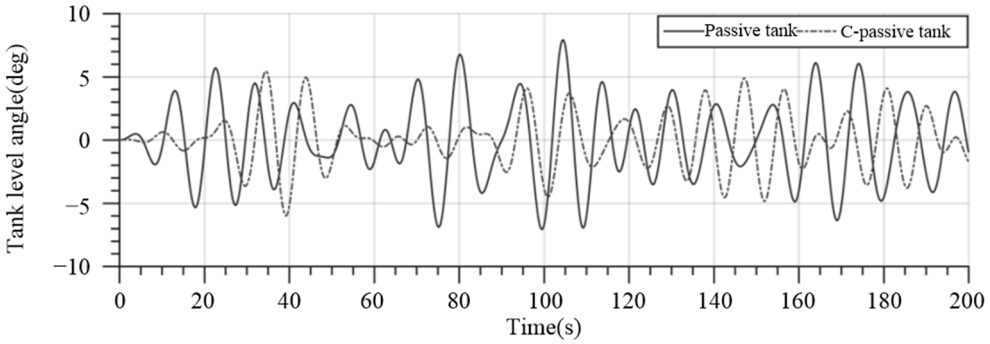

Figure 13. Tank level angle of passive anti-rolling tank and controllable passive anti-rolling tank.

Table 4. Maximum roll response data.

	Roll Angle (°)	Roll Rate (rad/s)	Tank Level Angle (°)
No tank	−5.15~5.02	−0.05777~0.05619	-
Passive anti-rolling tank	−3.00~3.85	−0.03945~0.03889	−7.07~7.91
Controllable passive anti-rolling tank	−2.14~2.35	−0.02798~0.02915	−6.00~5.44

When the gangway is overlapped with wind power piles under the condition of a significant wave height of 2.5 m, the probability that the roll angle and roll angular velocity of the ship exceed the movement range of the gangway on the ship when the ship is equipped with no tank, a passive anti-rolling tank, or a controllable passive anti-rolling tank is calculated as shown in Figure 14.

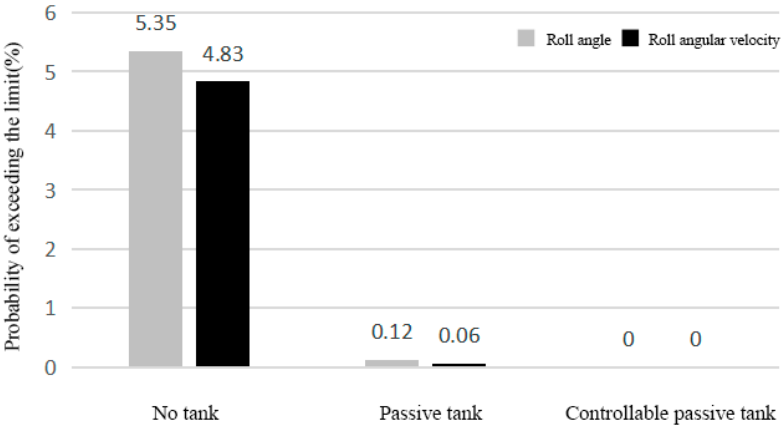

Figure 14. Probability of ship's roll angle and roll angular velocity exceeding the limit.

It can be seen from Figure 14 that under significant wave heights of 2.5 m, the probability that the roll angle and roll angular velocity of the ship equipped with an anti-rolling tank exceed the gangway movement limit on the ship is greatly reduced compared with the ship without an anti-rolling tank, and the probability of exceeding the limit is significantly reduced when the ship is equipped with a controllable passive anti-rolling tank.

4. Hardware-in-the-Loop Simulation

4.1. Control Architecture

The hardware-in-the-loop (HIL) simulation is used to verify the results. Six 750 W AC servo motors are used to drive the 6-DOF motion platform to simulate the hull movement. The picture of the 6-DOF motion platform is shown in Figure 15.

Figure 15. 6-DOF motion platform.

The control architecture of the hardware-in-the-loop simulation system is shown in Figure 16. The dashed box shows the real-time kernel running in the controller. The controller is connected to the servo driver of the 6-DOF motion platform through the Ether CAT bus, and connected to the gangway micro servo driver through the peripheral I/O module. The touch screen is selected as the development or expansion of the human–machine interface. The controller adopts Beckhoff's industrial PC, and Beckhoff's Twincat3 software supports the integration of MATLAB/Simulink; therefore, the Simulink model can be directly encapsulated and transplanted to the Twincat3 software platform for execution without intermediate secondary development. The real-time model of the ship with anti-rolling tank is built by the computer, and then integrated into the Twincat3 software platform. It forms a closed-loop system with the 6-DOF motion platform, attitude sensor, and gangway on the ship. In this way, the response time of the simulation program is consistent with the actual time, forming a real-time control system.

4.2. HIL Simulation Results

When the gangway end-effector is in the desired position, ΔL_1 and ΔL_2 are 25 mm and 24 mm, respectively. The HIL simulation results of the command length and speed of gangway telescopic rod and pitch rod under the condition of a significant wave height of 2.5 m and ship speed of 0 kn are shown in Figures 17–20.

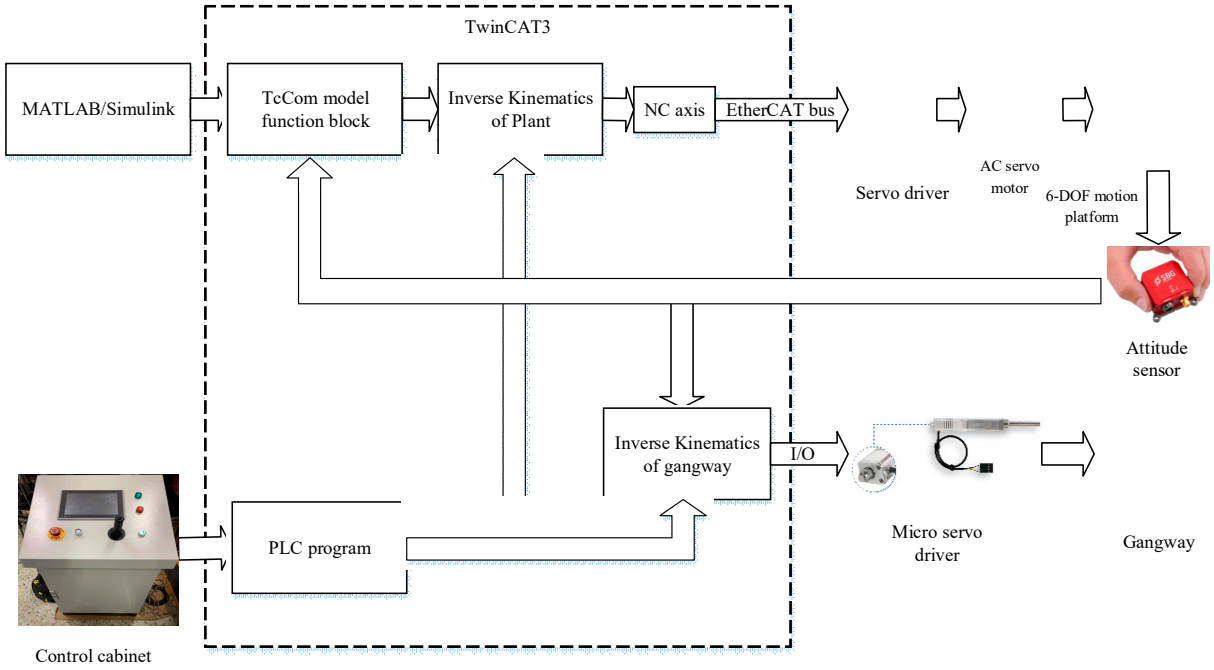

Figure 16. Control Diagram of the hardware-in-the-loop simulation system.

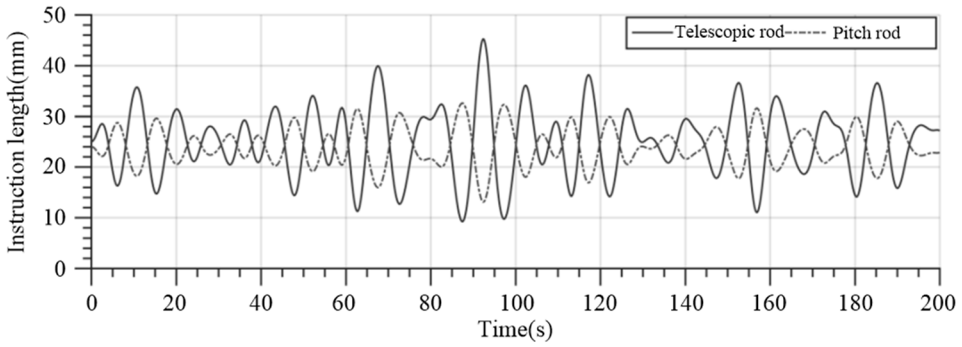

Figure 17. Command length of gangway telescopic rod and pitch rod when the ship is equipped with passive anti-rolling tank.

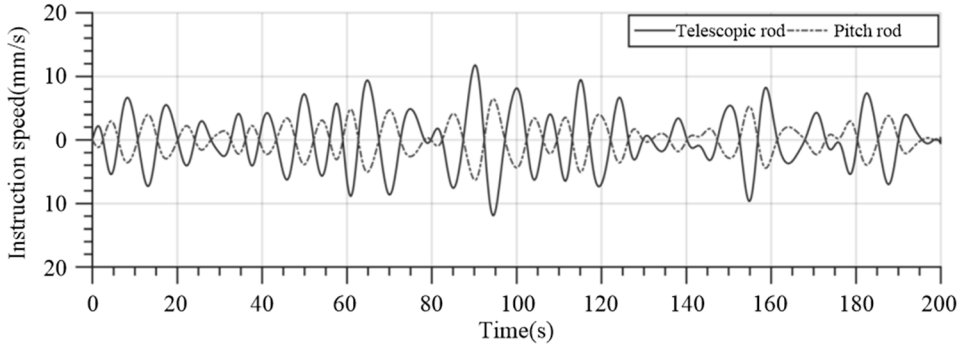

Figure 18. Command speed of gangway telescopic rod and pitch rod when the ship is equipped with passive anti-rolling tank.

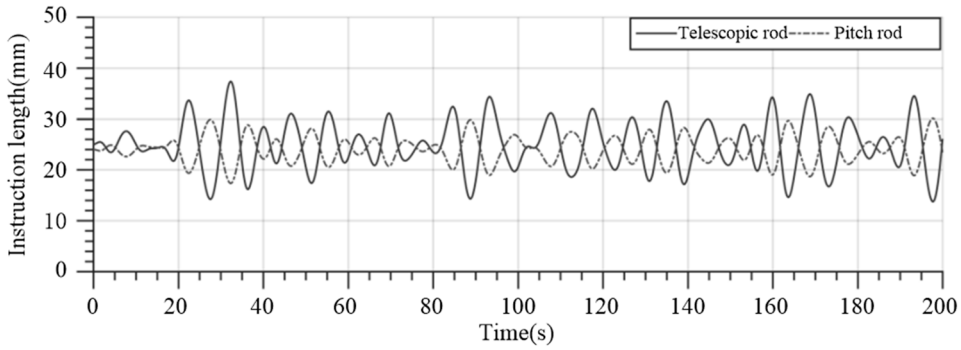

Figure 19. Command length of gangway telescopic rod and pitch rod when the ship is equipped with controllable passive anti-rolling tank.

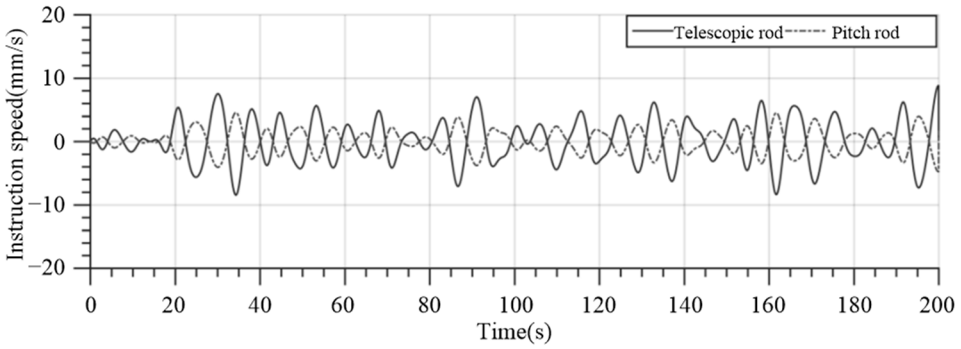

Figure 20. Command speed of gangway telescopic rod and pitch rod when the ship is equipped with controllable passive anti-rolling tank.

It can be seen from the HIL simulation results that the length and speed of the telescopic rod of the gangway exceed the motion limit because the roll amplitude and angular velocity of the ship exceed the motion limit in some roll periods when the ship is with no tank. However, when the ship is equipped with a passive anti-rolling tank or controllable passive anti-rolling tank, the active gangway compensation for ship motion is more ideal, and the length and speed of the telescopic rod and pitch rod are within the limit range.

Based on the gangway kinematic model established in Section 2, the end-effector trajectories with and without compensated ship motion over the gangway are simulated under random waves with a significant wave height of 2.5 m. The simulation results are shown in Figures 21–23. The hollow points in Figures 21–23 show the position trajectories of the gangway end-effector when the gangway compensation function is not enabled and only under the action of the passive anti-rolling tank and controllable passive anti-rolling tank, respectively. The solid points in Figures 21–23 show the position trajectories of the gangway end-effector under the combined action of the passive anti roll tank, controllable passive anti roll tank, and gangway compensation, respectively.

It can be seen from the HIL simulation results, the effect of the gangway on compensating the ship roll motion is poor. When the ship is equipped with a passive anti-rolling tank or a controllable anti-rolling tank, the gangway is ideal to compensate for the ship's motion. The compensation effect of a ship equipped with a controllable passive anti-rolling tank is better than that of a ship equipped with a passive anti-rolling tank. The HIL simulation results are consistent with the results in Section 3. It can be seen that the ship that is equipped with a controllable passive anti-rolling tank improves the accessibility of the gangway and ensures the safety of maintenance technicians.

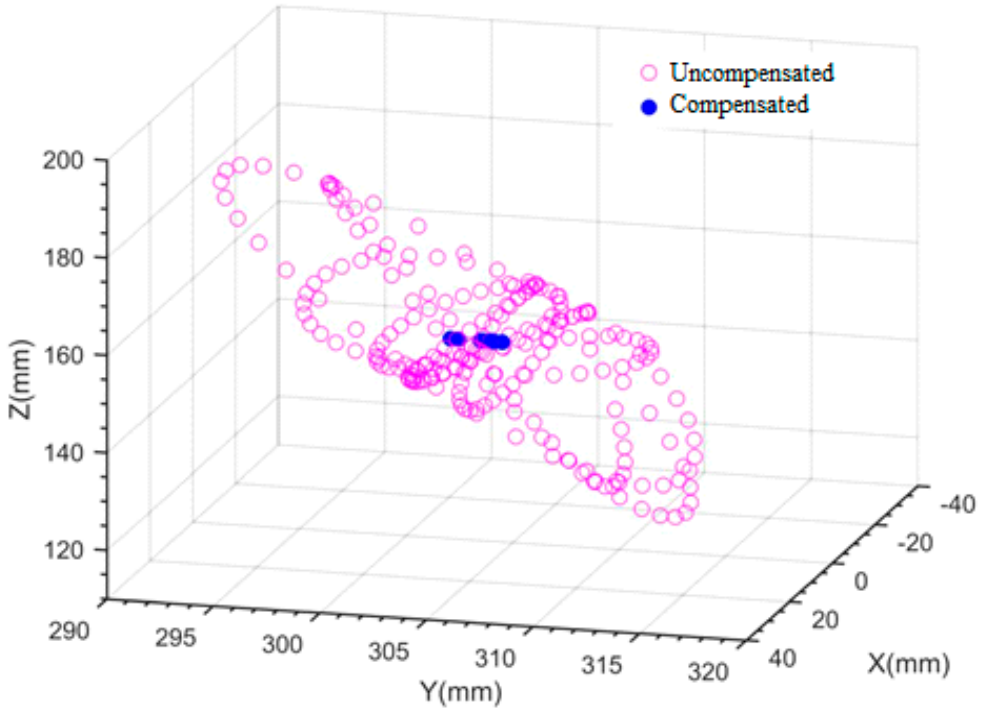

Figure 21. Comparison between uncompensated and compensated end effector trajectory when the ship is not equipped with an anti-rolling tank.

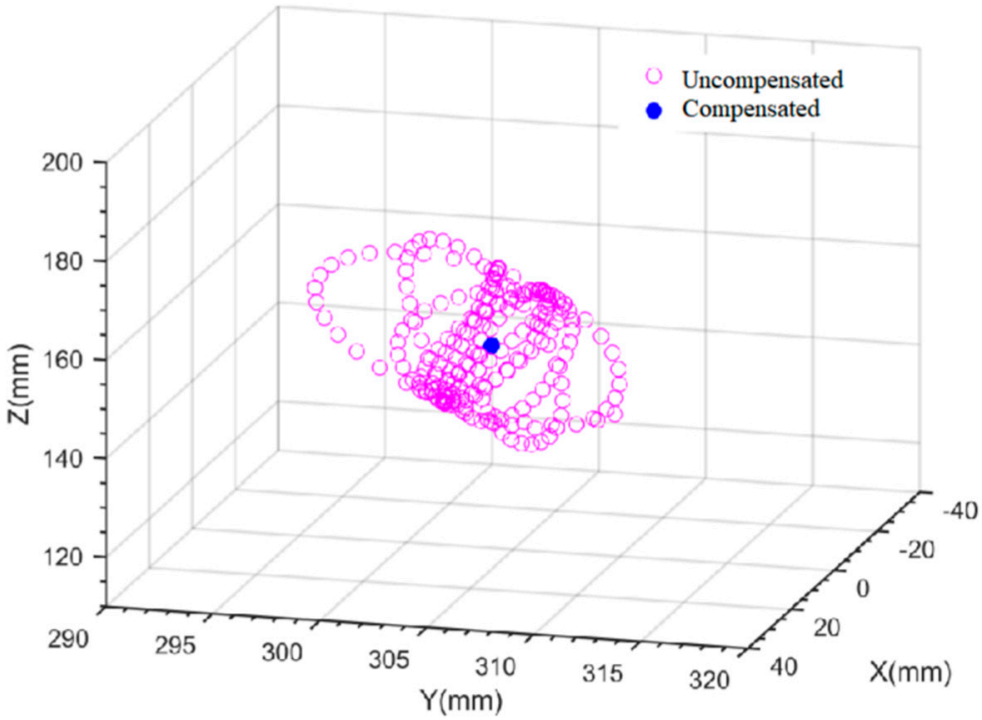

Figure 22. Comparison between uncompensated and compensated end effector trajectories when the ship is equipped with a passive anti-rolling tank.

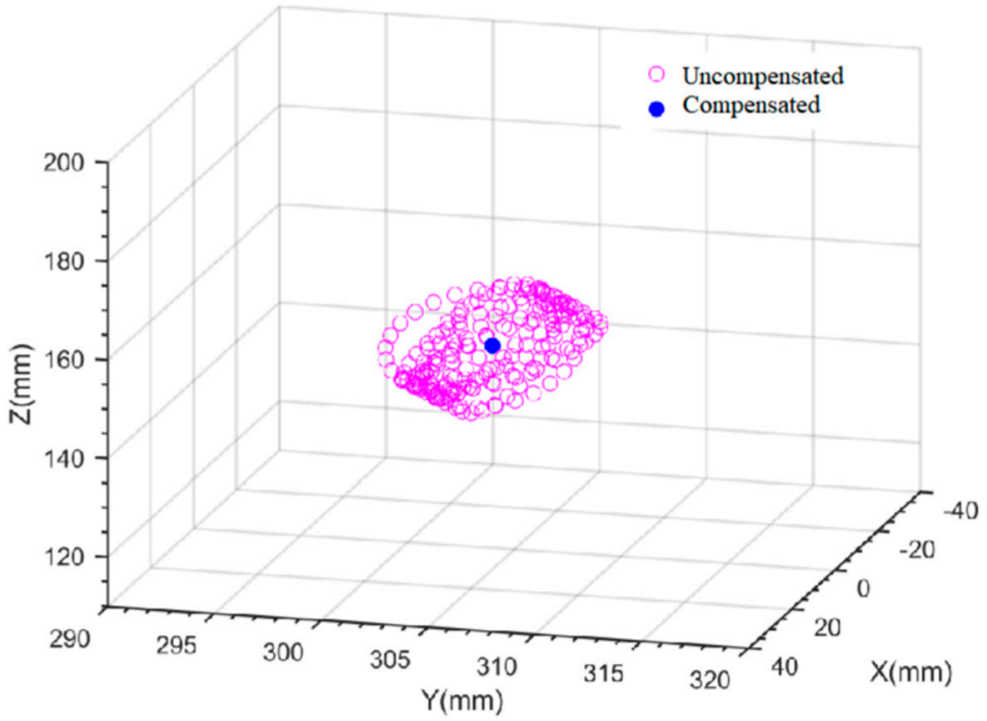

Figure 23. Comparison between uncompensated and compensated end effector trajectories when the ship is equipped with a controllable passive anti-rolling tank.

5. Conclusions

In this paper, the impact of an anti-rolling tank on accessibility of an offshore O&M gangway was investigated. The model of a ship's roll motion when coupled with a controllable passive anti-rolling tank is established, and the control method for the air valve is discussed. Taking a wind power operation and maintenance ship as the research object, a controllable passive anti-rolling tank with six air-valve channels was designed. The designed water tank was studied and analyzed by using the computational fluid dynamics software Ansys Fluent. In order to achieve better roll reduction effect, a period prediction algorithm based on wavelet neural network was proposed to predict the roll period of the target ship. The simulation results show that the proposed prediction algorithm can relatively accurately predict the roll period of the ship. On this basis, combined with the analysis of the motion of the on-board gangway, the impact of the anti-rolling tank on the gangway accessibility is discussed through simulation research. The simulation results show that the accessibility of the on-board gangway significantly improves when the ship is equipped with a controllable passive anti-rolling tank. Finally, the hardware-in-the-loop simulation of the active compensation gangway system was carried out. The simulation and test results show that the anti-rolling tank can effectively restrain the rolling motion of the ship, significantly improve gangway accessibility, and ensure the safety of maintenance technicians.

Author Contributions: Conceptualization, S.Z. and Z.S.; methodology, S.Z. and Z.S.; software, Z.S. and C.L.; validation, Z.S. and C.L.; formal analysis, Z.S.; investigation, Z.S. and C.L.; resources, S.Z.; data curation, Z.S.; writing—original draft preparation, P.Z., C.L. and Z.S.; writing—review and editing, P.Z. and S.Z.; visualization, S.Z. and P.Z.; supervision, S.Z.; project administration, S.Z.; funding acquisition, S.Z. and L.L. All authors have read and agreed to the published version of the manuscript.

Funding: This research was funded by the Doctorial Innovation Funds of Tangshan University under Grant 1402001, the Fundamental Research Funds for the Central Universities under Grants HEUCFM170404 and Harbin Science and Technology Innovation Talent Research Special Fund under Grant 2017RC2017XK009006.

Institutional Review Board Statement: Not applicable.

Informed Consent Statement: Not applicable.

Data Availability Statement: The authors confirm that the data supporting the findings of this study are available within the article.

Conflicts of Interest: The authors declare no conflict of interest.

References

1. Martin, J.; Atse, L. *Technological Learning in the Transition to a Low-Carbon Energy System*; Academic Press: Cambridge, MA, USA, 2020.
2. Matt, S.; Philipp, B.; Jake, N.; Aubryn, C.; Patrick, D. Impacts of turbine and plant upsizing on the levelized cost of energy for offshore wind. *Appl. Energy* **2021**, *298*, 117189.
3. Perez, T. *Ship Motion Control: Course Keeping and Roll Stabilisation Using Rudder and Fins*; Springer: London, UK, 2005.
4. Jin, H.; Yao, X. *Ship Control Principle*, 2nd ed.; Harbin Engineering University: Harbin, China, 2013.
5. Zhang, S.; Liang, L.; Sun, M.; Zhao, P. Fluid motion and stabilization effect prediction of anti-rolling tank coupled ship rolling. *Chin. J. Comput. Mech.* **2016**, *33*, 252–256+262.
6. Lewis, E. *Principles of Naval Architecture*, 2nd ed.; SNAME: New Jersey, NJ, USA, 1989; Volume 3.
7. Liang, L.; Zhao, P.; Zhang, S.; Yuan, J.; Wen, Y. Simulation and analysis of Magnus rotating roll stabilizer at low speed. *Ocean Eng.* **2017**, *142*, 491–500. [CrossRef]
8. Liang, L.; Jiang, Y.; Zhang, Q.; Le, Z. Aspect ratio effects on hydrodynamic characteristics of Magnus stabilizers. *Ocean Eng.* **2020**, *216*, 107699. [CrossRef]
9. Perez, T.; Blanke, M. Ship roll damping control. *Annu. Rev.* **2012**, *36*, 129–147. [CrossRef]
10. Fang, M.; Luo, J. On the track keeping and roll reduction of the ship in random waves using different sliding mode controllers. *Ocean Eng.* **2007**, *34*, 479–488. [CrossRef]
11. Liu, Z.; Jin, H.; Katebi, R. Ship forward speed loss minimization using nonlinear course keeping and roll motion controllers. *Ocean Eng.* **2016**, *113*, 201–207. [CrossRef]
12. Liang, L.; Wen, Y. Rudder roll stabilization with disturbance compensation model predictive control. *J. Mar. Sci. Technol.* **2018**, *24*, 249–259. [CrossRef]
13. Liang, L.; Zhao, P.; Zhang, S.; Ji, M.; Yuan, J. Simulation analysis of rudder roll stabilization during ship turning motion. *Ocean Eng.* **2019**, *189*, 106322.1–106322.11.
14. Zhang, Q.; Zhang, L.; Cao, K.; Xing, Y.; Wan, J. Design of u-type anti-rolling tank for Ultra-deepwater drillship. *J. Wuhan Univ. Technol.* **2019**, *43*, 271–350.
15. Wen, X.; Wan, D. Numerical simulation of liquid sloshing in anti-roll tank by MPS method. *Chin. J. Hydrodyn.* **2019**, *34*, 489–493.
16. Hu, J. *Study on Control Strategy of Anti-Rolling Tanks under Parametric Roll*; Harbin Engineering University: Harbin, China, 2019.
17. Luo, H.; Wang, C.; Sheng, Q. Numerical and model test on eigen characters of rolling motion of anti-rolling tank. *China Offshore Platf.* **2020**, *35*, 1–6.
18. Rahul, S.; Jyothish, P.; Anantha, S. Genetic Algorithm based design optimization of a passive anti-roll tank in a sea going vessel. *Ocean Eng.* **2020**, *203*, 107216.
19. Liang, L.; Wang, J.; Song, J.; Li, Y. Design and simulation investigation of variable period passive anti-rolling tank. *Chin. J. Ship Res.* **2021**, *16*, 147–154.
20. Immink, L. *Feed forward Control of U Anti-Roll Tanks*; University Science: Mill Valley, CA, USA, 2021.
21. Lloyd, A. *Seakeeping: Ship Behaviour in Rough Weather*; Ellis Horwood: Chichester, UK, 1989.
22. Gawad, A.; Ragab, S.; Nayfeh, A.; Mook, D. Roll stabilization by anti-roll passive tanks. *Ocean Eng.* **2001**, *28*, 457–469. [CrossRef]
23. Jin, H.; Zhang, H. Research on pneumatical-passively-controlled tank stabilizers based on GPC strategy. *Shipbuild. China* **2010**, *51*, 67–75.
24. Zhao, Y.; Yang, Q.; Su, D.; Zou, L.; Wang, A. Rogue wave prediction based on wavelet neural network. *J. Harbin Inst. Technol.* **2021**, *53*, 112–117.
25. Zhang, S. Characteristics Research and Experimental Verification of Controlled Passive Tank. Ph.D. Thesis, Harbin Engineering University, Harbin, China, 2013.